CHEMISTRY
A EUROPEAN JOURNAL

DOI: 10.1002/chem.201003672

Regular Acyclic and Macrocyclic [AB] Oligomers by Formation of Push–Pull Chromophores in the Chain-Growth Step

Fabio Silvestri,[a] Markus Jordan,[a] Kara Howes,[a] Milan Kivala,[a] Pablo Rivera-Fuentes,[a] Corinne Boudon,[b] Jean-Paul Gisselbrecht,[b] W. Bernd Schweizer,[a] Paul Seiler,[a] Melanie Chiu,[a] and François Diederich*[a]

Dedicated to Professor Didier Astruc on the occasion of his 65th birthday

Abstract: The substrate scope of the [2+2] cycloaddition–cycloreversion (CA–CR) reaction between electron-deficient (2,2-dicyanovinyl)benzene (DCVB) or (1,2,2-tricyanovinyl)benzene (TCVB) derivatives and *N*,*N*-dimethylanilino (DMA)-substituted acetylenes was investigated. The structural features of the cyanobutadiene products of these transformations were examined and the rates of selected CA–CR reactions were measured. Rate constants for reactions utilizing pentafluorinated TCVB and DCVB were found to be one to two orders of magnitude larger than those for the unsubstituted analogues. Multiple, consecutive CA–CR reactions were performed with substrates incorporating two reactive 2,2-cyanovinyl or 4-ethynylanilino sites. 1,4-Bis(2,2-dicyanovinyl)-2,3,5,6-tetrafluorobenzene and 1,4-bis[(4′-dihexylamino)phenylethynyl]benzene were selected as suitably reactive monomers for the synthesis of regular [AB] oligomers wherein the push–pull chromophores were formed in the chain-growth step. Oligomers of two types were isolated: macrocyclic $[AB]_n$ and open-chain $B[AB]_n$ oligomers, with $n \leq 4$.

Keywords: cycloaddition–cycloreversion · chromophores · cyclophanes · donor–acceptor systems · oligomerization

Introduction

Nonplanar, π-conjugated, donor–acceptor chromophores that feature low-energy charge-transfer (CT) absorptions are attractive materials for nonlinear optical and photonic applications.[1] One particularly efficient method for accessing these chromophores is a formal [2+2] cycloaddition–cycloreversion (CA–CR) reaction between electron-rich alkynes, such as *N*,*N*-dialkylanilino (DAA)-substituted acetylenes, and electron-deficient alkenes, such as tetracyanoethene (TCNE), yielding nonplanar donor-substituted cyanobuta-1,3-dienes that feature intense, bathochromically shifted, intramolecular CT bands.[2,3] Apart from the excellent optoelectronic performance and demonstrated utility of the push–pull chromophore products,[4,5] the reaction typically proceeds rapidly and with very good yields. These properties stimulated us to explore the use of the CA–CR transformation for the preparation of regular push–pull oligomers, which may ultimately lead to the synthesis of polymers and dendrimers.

One possibility for accessing push–pull-chromophoric polymers by means of the CA–CR transformation has been reported by Michinobu and co-workers: polymers are synthesized with donor-activated acetylene moieties either in the main chain or laterally appended; these acetylene moieties subsequently undergo reaction with tetracyanoethene (TCNE) as a post-polymerization modification.[6] Another, hitherto unexplored possibility for accessing regular [AB] oligomers utilizing this reaction enables the formation of push–pull chromophores in the chain-growth step. Such an approach can be realized if both monomers, A and B, are able to participate in multiple, consecutive CA–CR reactions.[7] Recently, weaker acceptors, such as 2,2-dicyanovinylbenzene (DCVB) and 1,2,2-tricyanovinylbenzene (TCVB) derivatives were found to be capable of undergoing the CA–CR reaction in high yields and with complete diastereoselectivity.[8] This discovery prompted us to explore the use of bis(dicyanovinyl)benzene (bis(DCV)) and bis(tricyanovinyl)benzene (bis(TCV)) derivatives as A monomers in the synthesis of [AB] oligomers (Scheme 1).

Because a high-yielding and facile chain-growth step is imperative to access oligomers, and eventually longer poly-

[a] Dr. F. Silvestri, Dr. M. Jordan, Dr. K. Howes, Dr. M. Kivala, P. Rivera-Fuentes, Dr. W. B. Schweizer, P. Seiler, Dr. M. Chiu, Prof. Dr. F. Diederich
Laboratorium für Organische Chemie, ETH Zürich
Hönggerberg, HCI, 8093 Zürich (Switzerland)
Fax: (+41) 44-632-1109
E-mail: diederich@org.chem.ethz.ch

[b] Prof. Dr. C. Boudon, Dr. J.-P. Gisselbrecht
Laboratoire d'Electrochimie et de Chimie Physique
du Corps Solide, Institut de Chimie
UMR 7177, C.N.R.S., Université de Strasbourg
4, rue Blaise Pascal, CS 90032
67081 Strasbourg Cedex (France)

Supporting information for this article is available on the WWW under http://dx.doi.org/10.1002/chem.201003672.

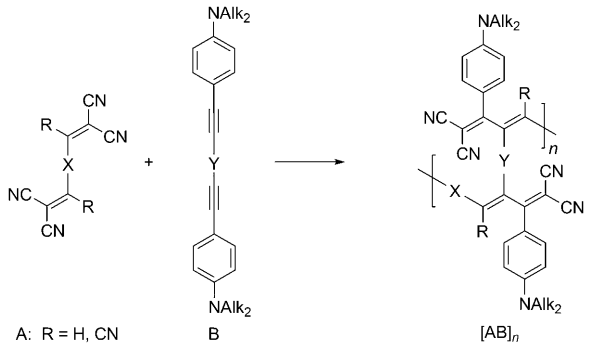

Scheme 1. Formation of [AB] oligomers by using the CA–CR reaction to install push–pull chromophores in the chain-growth step. X and Y can be a variety of spacers; Alk is an alkyl chain.

mers, we initiated our studies with a series of model reactions and kinetic studies designed to determine the degree to which the DCVB or TCVB acceptors should be activated to attain optimal reactivity. X-ray crystallographic studies on the cyanobutadiene products of these model reactions suggest that the reactions proceed through a highly torquoselective, cyclobutene-opening step. Subsequently, donors and acceptors incorporating two reactive sites were shown to undergo multiple, consecutive CA–CR reactions. Finally, we translated the findings from these model studies to the synthesis of a new class of regular acyclic and macrocyclic [AB] oligomers.

Results and Discussion

Model studies for identifying an A monomer: To identify the optimal acceptor motif for the A monomer to be used in the targeted oligomerization reactions (Scheme 1), a series of aryl-substituted DCVBs (**1**) and TCVBs (**2**) were prepared (see the Supporting Information). Their conversions in the CA–CR reaction with *N*,*N*-dimethylanilino- (DMA-) substituted terminal (**3**) and internal (**4**) acetylenes to afford donor-substituted cyanobutadienes **5–8** were investigated (see Scheme 2 and Table S1 in the Supporting Information for details). In contrast to reactions utilizing unsubstituted analogues **1a** and **2a** (for depiction, see Table 1), reactions using DCVBs and TCVBs that included electron-withdrawing substituents on the aryl ring (e.g., **1b–d** and **2b–d**) were uniformly high yielding.

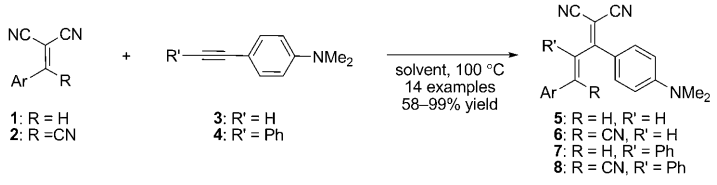

Scheme 2. CA–CR reactions of DCVBs and TCVBs with DMA-activated terminal and internal alkynes. Solvent = 1,1,2,2-tetrachloroethane or *N*,*N*-dimethylformamide.

To quantify whether the rates of CA–CR reactions with electronically activated acceptors are accelerated, kinetic studies were undertaken. We were particularly interested in the reactivity of pentafluorinated compounds **1b** and **2b** because reactions utilizing these compounds provided the best compromise between high yields and short reaction times. DCVBs **1a** and **1b** or TCVBs **2a** and **2b** were treated with DMA-acetylene **3** in $(CDCl_2)_2$ at 22 °C and the transformations were monitored by ^{1}H NMR spectroscopy (Table 1).

Table 1. Kinetic data from ^{1}H NMR spectroscopy of CA–CR reactions with unsubstituted and fluorinated DCVBs and TCVBs.[a]

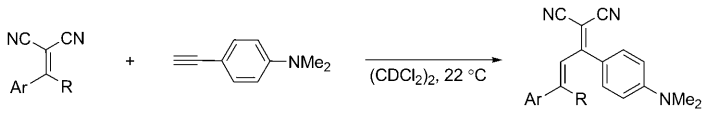

1: R = H
2: R =CN

3

5: R = H
6: R = CN

Entry	DCVB/TCVB	Product	k_{obs} [$M^{-1}s^{-1}$]	$t_{1/2}$ [min]
1[b]	**1a** Ar = Ph	**5a**	5.67×10^{-5}	8790
2	**1b** Ar = F_5Ph	**5b**	$(1.78\pm0.08)\times10^{-2}$	26.8 ± 1.6
3	**2a** Ar = Ph	**6a**	$(8.45\pm0.38)\times10^{-4}$	589 ± 24
4	**2b** Ar = F_5Ph	**6b**	$(1.28\pm0.06)\times10^{-2}$	42.7 ± 2.4

[a] Unless otherwise noted, reported values are the averages of three independent measurements; reported errors represent standard deviations. Initial concentration of all reagents was 0.032 M in $(CDCl_2)_2$ with hexamethylbenzene (0.011 M) as an internal standard; reactions were performed at 22 °C. [b] Reaction was performed once; reported values are extrapolated from initial rate measurement in which the reaction was followed to 25% conversion.

All reactions exhibited overall second-order behavior (see Figures S26–33 in the Supporting Information for detailed kinetic data and linear fits).[8b] While the rate constant (k_{obs}) for the reaction using fluorinated DCVB **1b** was $((1.78\pm0.08)\times10^{-2})\,M^{-1}s^{-1}$, the rate constant for transformation of unsubstituted DCVB **1a** was more than two orders of magnitude smaller ($k_{obs}=(5.67\times10^{-5})\,M^{-1}s^{-1}$). Similar behavior was observed in the TCVB systems: $k_{obs}=((1.28\pm0.06)\times10^{-2})$ and $((8.45\pm0.38)\times10^{-4})\,M^{-1}s^{-1}$ for the reactions utilizing perfluorinated TCVB **2b** and unsubstituted TCVB **2a**, respectively. It is noticeable that the third vinylic CN group in the TCVBs either inhibits or does not markedly facilitate conversion compared with reactions utilizing DCVBs (Table 1, entry 1 vs. 3 and entry 2 vs. 4). The increased electronic activation in the TCVBs is presumably mitigated by increased steric bulk; previous mechanistic studies indicate that the free enthalpy of activation ($\Delta G^{\neq}$) of the first [2+2] cycloaddition step is strongly increased by steric hindrance.[8b]

Characterization of DMA-substituted di- and tricyanobuta-1,3-dienes: X-ray crystallographic studies performed on single crystals of several cyanobutadiene products (for ORTEP plots, see Figures S34–45 in the Supporting Information) revealed two significant results: 1) the configuration of the TCVB-derived cyanobutadiene products was elucidated and 2) a correlation between steric bulk and effective

conjugation within the cyanobutadiene products was established. The CA–CR reactions of TCVBs with both terminal and internal DMA-substituted alkynes, such as those utilizing DCVBs,[8] yielded one diastereoisomer exclusively. Crystal structures of these products show that the aryl ring (from the TCVB precursor) and the dicyanovinyl moiety are *trans* oriented (**6b** and **8c** in Figure 1; for **6a**, see Figure S39 in the Supporting Information); this configuration is consistent with that observed for DCVB-derived cyanobutadienes (e.g., **5b**, **5d**, **7b**, and **7c** in Figures S37, 38, 42 and 43, respectively, in the Supporting Information).[8] These crystal structures constitute the first examples of donor-substituted tricyanobuta-1,3-dienes derived from TCVB precursors. The diastereoselectivity of this reaction testifies to the high torquoselectivity with which the cyclobutene intermediate opens.[9]

The structural parameters summarized in Table 2 show a correlation between steric bulk and conjugation within the cyanobutadiene monoadducts. With increasing steric bulk about the butadiene moiety, the dihedral angle θ, defined by the butadiene moiety (C4-C3-C5-C6, Table 2), increases. Thus, values of θ are smallest for cyanobutadienes **5b** (18.9(4)°) and **5d** (13.4(3)°) (Table 2, entries 1 and 2), which are formed from the terminal alkyne **3** and DCVBs **1b** or **1d**. More significant deviations from planarity, up to $\theta =$ 77.0(7)° (**6b**, entry 4), are found in the products obtained from the reaction of TCVBs **2a–d** and/or internal alkyne **4** (entries 4–9).

Increasing values of θ generally correlate to decreasing values of ϕ, the dihedral angle (C1-C2-C3-C4, Table 2) defined by the two vinylic C atoms of the dicyanovinyl (DCV) moiety and the two adjacent C(sp^2) atoms of the DMA moiety. Thus, increasing steric bulk about the butadiene moiety appears to induce the DMA and DCV moieties to approach coplanarity. These moieties are, in turn, responsible for the intramolecular CT in the chromophores,[2f] which is manifested in the solid state as bond-length alternation within the aniline rings (δr, see Table 2 for definition).[10] In sterically encumbered **7b**, δr is relatively strong (0.041 Å, Table 2, entry 6) in comparison with **5b** ($\delta r = 0.023$ Å) and **5d** ($\delta r = 0.016$ Å) (Table 3, entries 1 and 2). This large δr value in **7b** is consistent with more efficient conjugation between the DMA and DCV moieties, which is enabled by a relatively small value of ϕ (26.4(5)°). Putting these trends together, increasing steric bulk about the cyanobutadiene moiety ultimately translates to increasing conjugation and CT within cyanobutadiene chromophores.

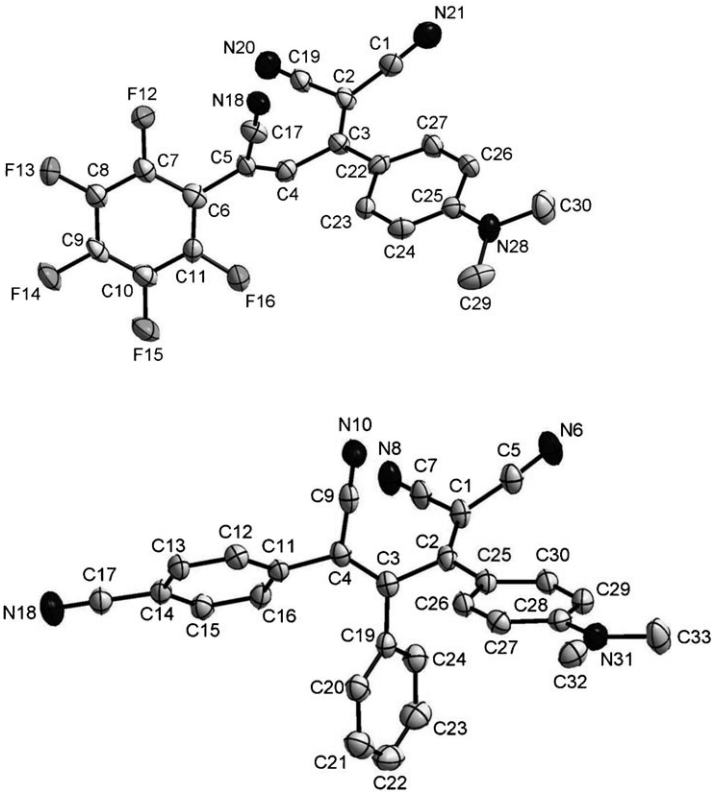

Figure 1. ORTEP representations of the molecular structures of **6b** (top, 220 K) and **8c** (bottom, 123 K). Thermal ellipsoids are shown at the 50% probability level. Hydrogen atoms are omitted for clarity and atoms are numbered arbitrarily. For selected bond lengths and angles, see the Supporting Information.

Table 2. Dihedral angles and bond-length alternation parameters from X-ray crystal structures for DMA-substituted cyanobutadiene chromophores.

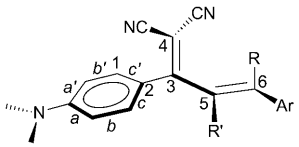

5: R = H, R' = H
6: R = CN, R' = H
7: R = H, R' = Ph
8: R = CN, R' = Ph

Entry	Compound	Ar	R	R′	θ [°][a]	ϕ [°][b]	δr [Å][c]
1	**5b**	F_5Ph	H	H	18.9(4)	48.7(4)	0.023
2	**5d**	4-CF_3-Ph	H	H	13.4(3)	47.0(3)	0.016
3	**6a**	Ph	CN	H	50.1(2)	37.5(2)	0.039
4	**6b**	F_5Ph	CN	H	77.0(7)	4.0(10)	0.03
5	**7a**	Ph	H	Ph	56.8(2)	26.9(3)	0.042
6	**7b**	F_5Ph	H	Ph	74.6(6)	26.4(5)	0.041
7	**7c**	4-CN-Ph	H	Ph	70.0(2)	28.5(3)	0.035
8	**7d**	4-CF_3-Ph	H	Ph	67.0(3)	26.6(3)	0.037
9	**8c**	4-CN-Ph	CN	Ph	70.9(4)	28.7(5)	0.039

[a] θ is the dihedral angle defined by C4-C3-C5-C6. [b] ϕ is the dihedral angle defined by C1-C2-C3-C4. [c] $\delta r = \{[(a+a')/2\text{-}(b+b')/2]+[(c+c')/2\text{-}(b+b')/2]\}/2$; for benzene, $\delta r = 0.00$ Å; for fully quinoid rings, $\delta r =$ 0.08–0.12 Å.

Table 3. Consecutive CA–CR reactions starting from **9** with two DAA-activated internal acetylenes.

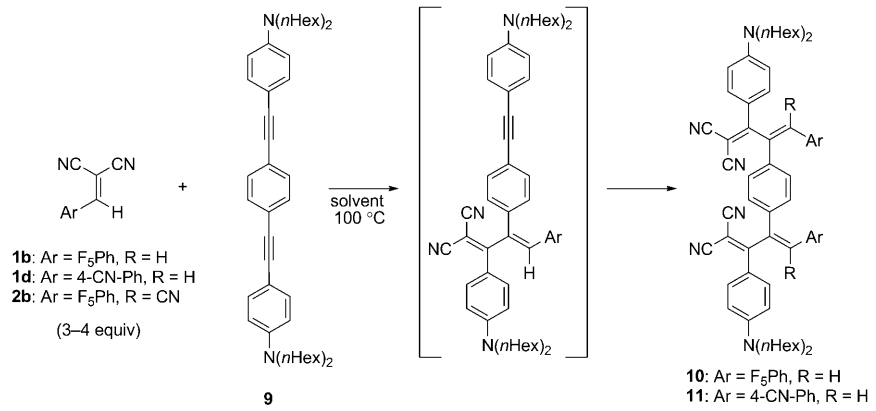

Entry	DCVB/TCVB	Solvent	Product	t [h]	Yield [%]
1	**1b** (3 equiv)	DMF[a]	**10**	18	37
2	**1c** (4 equiv)	DMF[a]	**11**	22	98
3	**2b** (3 equiv)	TCE[b]	–	24	–

[a] [**9**] = 0.01 M. [b] [**9**] = 0.04 M.

The UV/Vis and electrochemical properties of the new cyanobutadiene monoadducts obtained from these model studies are reported in the Supporting Information.

Consecutive CA–CR model studies: The reactivities of compounds with either two DAA-acetylene- or two DCV-/TCV-(tricyanovinyl-) reactive sites were evaluated. When bis(DAA-acetylene) derivative **9** was treated with excess pentafluorinated DCVB **1b** (3 equiv), the expected bisadduct was formed, but the reaction did not proceed to completion (Table 3). Formation of the monoadduct was observed by ^{1}H NMR spectroscopy, but the resulting deactivation of the second alkyne rendered the second addition very slow. Bisadduct **10** was only isolated in 37% yield after 18 h (DMF, 100°C). In contrast, a *p*-CN substituent on the phenyl ring of DCVB **1c** did not seem to influence the second addition to the same extent: bisadduct **11** was isolated in 98% yield. Its structure was confirmed by X-ray analysis (Figure 2) and indicated that the absolute torquoselectivity of the cyclobutene-ring-opening step is maintained in multiple-adduct formations: the 4-cyanophenyl and the dicyanovinyl moieties are *trans* oriented with respect to the C4=C5 double bond. Each of these reactions yields the product as only a single diastereomer. UV/Vis spectroscopy and electrochemical data for bisadducts **10** and **11** are included in the Supporting Information (Figure S50 and Table S2, respectively). In the reaction utilizing TCVB **2b**, only monoadduct and no desired bisadduct were obtained. The additional CN group deactivates the remaining, directly π-conjugated acetylene bond in the monoadduct, rendering it inert to further reaction.

Both non-[11] and tetrafluorinated bis(2,2-dicyanovinyl)-benzene (**12a** and **12b**, respectively) and bis(1,2,2-tricyanovinyl)benzene derivatives (**13a** and **13b**) (see the Supporting Information for the synthesis of **12b** and **13b**) underwent two, consecutive CA–CR reactions with DMA-acetylene **3**, providing, in most cases, very good yields of corresponding bisadducts **14a**, **14b**, **15a**, and **15b** in short reaction times (see Table 4, entries 1 and 4). Because the push–pull chromophore formed in the first addition remains a potent electron acceptor,[2] the monoadduct is sufficiently activated for the second addition step. The reaction of **3** and **13a** to form bisadduct **15a** was monitored by ^{1}H NMR spectroscopy (see Figure S25 in the Supporting Information): after 20 h at 100°C, 50% conversion to the intermediate monoadduct and 45% conversion to the bisadduct were observed, in addition to trace amounts of the starting material.

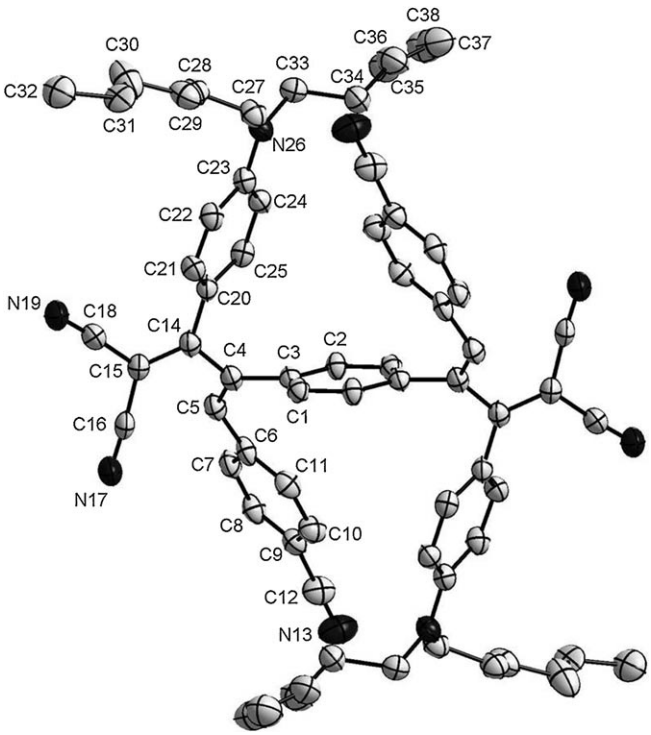

Figure 2. ORTEP representation of the molecular structure of **11** in the crystal (123 K). Thermal ellipsoids are shown at the 50% probability level. Hydrogen atoms and minor occupations of disordered atoms (C31 and C32) are omitted for clarity and atoms are numbered arbitrarily. Selected bond lengths [Å] and dihedral angles [°]: C23–C24 1.411(5), C24–C25 1.377(5), C25–C20 1.408(6), C20–C21 1.399(5), C21–C22 1.383(5), C22–C23 1.419(6), C20–C14 1.455(5), C14–C15 1.378(6), C14–C4 1.482(5), C4–C5 (1.346(5), C4–C3 1.490(4), C5–C6 1.465(5); C3-C4-C5-C6 −11.4(6), C5-C4-C14-C15 −46.8(5), C15-C14-C20-C21 −37.2(5).

These data show that bis-additions to both bis(DAA-alkyne) and bis(DCV) or bis(TCV) substrates are possible,

Table 4. Consecutive CA–CR reactions starting from 1,4-bis(2,2-dicyanovinyl)- and bis(1,2,2-tricyanovinyl)-benzene derivatives.

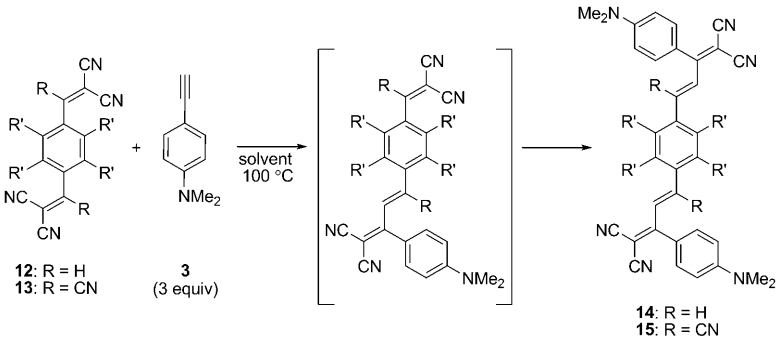

Entry	Cyanoolefin	Solvent	Product	t [h]	Yield [%]
1	**12a** R′=H	DMF	**14a**[a]	5	86
2	**12b** R′=F	DMF	**14b**[a]	15	70
3	**13a** R′=H	TCE	**15a**[b]	72	94
4	**13b** R′=F	TCE	**15b**[a]	1	95

[a] [Cyanoolefin] = 0.02 M. [b] [Cyanoolefin] = 0.006 M.

with the DCV derivatives performing better than the TCV derivatives in many cases, presumably due to a combination of steric and electronic effects.

Synthesis, isolation, and characterization of [AB] oligomers: Bis(DCV) derivative **12b** (A, see Scheme 3) was reacted with bis(DAA-alkyne) derivative **9** (B) in TCE at 80 °C. The transformation was monitored by using MALDI-TOF mass spectrometry. Consumption of the 1,4-bis(phenylethynyl)-benzene starting material, **9**, and concomitant formation of a mixture of oligomeric products (Scheme 3) were observed. The signals in the mass spectrum of the crude product mixture correspond to m/z values that are consistent with products of three general formulae: $[AB]_n$ (**16a–d**) and $B[AB]_n$ (**17a–d**), in which n = 1–4, as well as $A[AB]_n$ (**18**), in which n = 1–3 (see Figure S52 in the Supporting Information for the mass spectrum of the crude reaction mixture). Recycling gel permeation chromatography (GPC) was performed to separate the components of the product mixture (for their mass spectra, see the Supporting Information). Samples of $[AB]_n$ (n = 2–4) and $B[AB]_n$ (n = 1–4) oligomers were isolated with $[AB]_2$ oligomer **16b** procured, by far, as the major product (21 %). The second-most-abundant compound isolated was $B[AB]_1$ oligomer **17a** (2 %). These two major isolated products were fully characterized by NMR spectroscopy (^{1}H, ^{13}C, and ^{19}F; see the Supporting Information). Interestingly, the reaction of **9** with bis(TCV) derivative **13b** did not afford any higher oligomeric products and only formation of a monoadduct was observed.

Signals in the NMR spectra of the major product, $[AB]_2$ oligomer **16b**, were sharp at room temperature and were indicative of a molecule with apparent D_{2h} symmetry. These observations led us to postulate that **16b** was macrocyclic in structure. To test this hypothesis, we treated **16b** with a further two equivalents of DCVB **1b** under the oligomerization reaction conditions; no reaction was observed by MALDI-TOF mass spectrometry, which was consistent with a cyclic structure that did not contain free, reactive acetylene groups. When $B[AB]_1$ oligomer **17a** was treated with DCVB **1b**, however, consumption of starting material was observed by ^{1}H NMR spectroscopy, suggesting that **17a** possessed an open-chain connectivity.

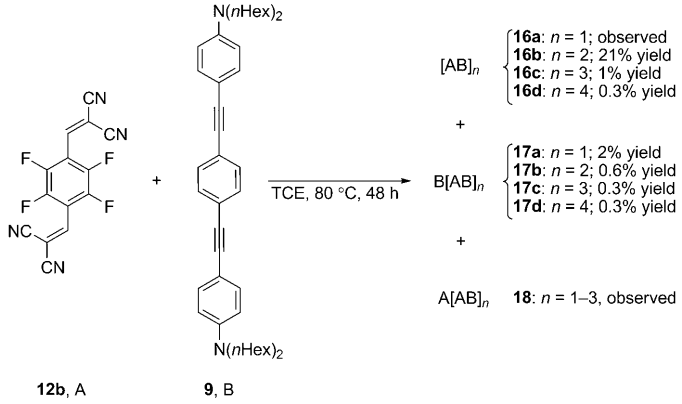

Scheme 3. CA–CR oligomerization reaction between **12b** (monomer A, see Scheme 1) and **9** (monomer B) in TCE. Reaction conditions: [**9**] = 0.02 M in TCE, **12b** (1 equiv). Unoptimized yields are reported.

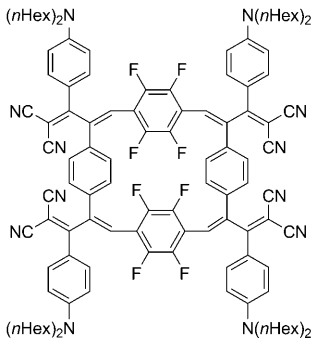

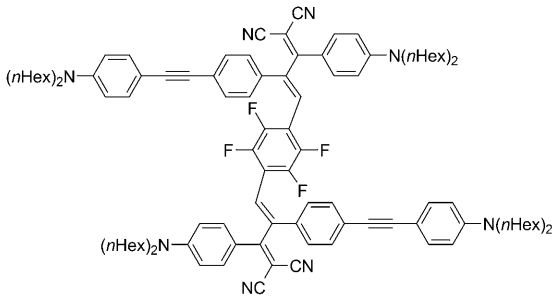

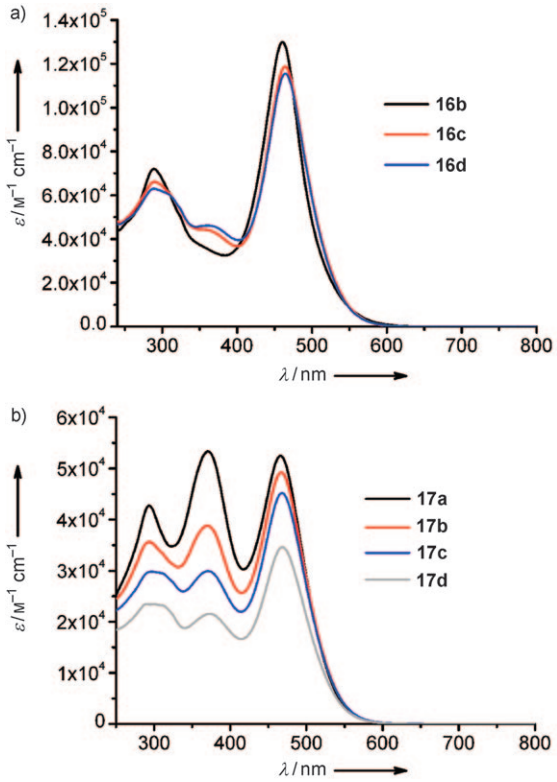

Figure 3. UV/Vis spectra of a) cyclic $[AB]_n$ and b) acyclic $B[AB]_n$ oligomers isolated from the CA–CR oligomerization of **9** and **12b** (CH_2Cl_2, 298 K).

The UV/Vis spectra of **16b** and **17a**, as well as the isolated higher-order $[AB]_n$ and $B[AB]_n$ oligomers provided further insight into the structures of these compounds (Figure 3). The longest-wavelength maxima in both series appear at about 470 nm and do not change with oligomer length. The homology between the UV/Vis spectra of **16b** and the higher-order $[AB]_n$ oligomers, **16c** and **16d**, suggests that these compounds are possibly all cyclic in structure. Additionally, the molar extinction coefficients in the $[AB]_n$ oligomers do not increase with increasing oligomer size. The larger compounds become more fluxional, as evident from the broadness of the signals in the NMR spectra. Analogously, the similarities between the UV/Vis spectra of **17a** and the higher-order $B[AB]_n$ oligomers suggest that these compounds are of an open-chain connectivity. Whereas the absorption strengths of all compounds in the $[AB]_n$ series are similar (Figure 3a), the molar extinction coefficients of the three absorption bands in the $B[AB]_n$ oligomers decrease with increasing oligomer length (Figure 3b). We speculate that this strong hypochromicity might arise from arene–arene interactions in a helical or folded conformation in these oligomers.[12] Two additional observations are consistent with this tentative hypothesis: 1) the sharpness of all three absorption bands remains constant, and 2) bisadduct **11** possesses a bent "H" structure in the solid state (Figure 2).

The CT character of the longest-wavelength absorptions of the $[AB]_n$ and $B[AB]_n$ oligomers was demonstrated in reversible protonation–deprotonation experiments (see Figure S51 in the Supporting Information). When $B[AB]_1$ oligomer **17a** was treated with excess trifluoroacetic acid (TFA), the two lower-energy absorption bands at about 380 and 470 nm disappeared. Subsequent addition of triethylamine to the sample resulted in the reappearance of both absorption bands. Thus, both absorption bands can be ascribed to intramolecular CT in the $B[AB]_n$ oligomers. To distinguish the two CT interactions from one another, TFA (0.4 equiv) was added to B[AB] oligomer **17a**, causing only the absorption band at around 380 nm to disappear. Because the anilino moieties that are conjugated to the alkyne unit are more basic than those adjacent to the DCV groups, the absorption band at about 380 nm can be attributed to an intramolecular CT from the DAA-acetylene to the adjacent DCV moiety. In $[AB]_2$ oligomer **16b**, only one type of DAA moiety is present, and the protonation–deprotonation experiments identified only the strong absorption maximum at around 470 nm as a CT band.

Computational studies corroborated the proposed connectivity of $[AB]_2$ oligomer **16b** and yielded insight into its electronic structure (see the Experimental Section for details). A simplified analogue of the proposed cyclic oligomer **16b**, wherein the hexyl chains on the aniline nitrogen atoms were replaced with methyl groups, was subjected to conformational analysis. A global minimum was identified and further optimized at the B3LYP/6-31G(d) level of theory (see Figure S60 in the Supporting Information). This conformation is C_2 symmetric. However, all aromatic rings rotate freely according to molecular dynamics simulations, leading to a higher pseudo-symmetry that is consistent with the experimental NMR spectrum of **16b**. Furthermore, the UV/Vis spectrum of **16b** was simulated by using the structure of the calculated global minimum, wherein vertical excitations were simulated at the time-dependent (TD) CAM-B3LYP/6-31G(d) level of theory. Good agreement between the simulated and experimental spectra of **16b** (see Figure S61 in the Supporting Information) further supports the proposed macrocyclic structure of that compound. The calculated UV/Vis spectrum of acyclic $B[AB]_1$ oligomer **17a** (see Figure S62 in the Supporting Information) also agrees with its experimental spectrum, which validates the use of these calculations for predicting the connectivity of the oligomers.

Finally, the origin of the single CT absorption band observed in the UV/Vis spectrum of cyclic $[AB]_2$ oligomer **16b** was elucidated by molecular orbital calculations. The highest occupied molecular orbitals (HOMO-3 to HOMO) for cyclic oligomer **16b** include two pairs of degenerate orbitals centered on the four aniline rings (Figure 4a and b). This degeneracy lends further credence to the proposed cyclic structure of **16b** because an open-chain structure is of lower symmetry and such degeneracy would not be possible. Furthermore, the fact that these four HOMO orbitals are close in energy is consistent with the unique four-electron oxidation at +0.74 V observed in the cyclic voltammogram of **16b** (see Figure S46 in the Supporting Information). The electron density of the calculated first four virtual orbitals

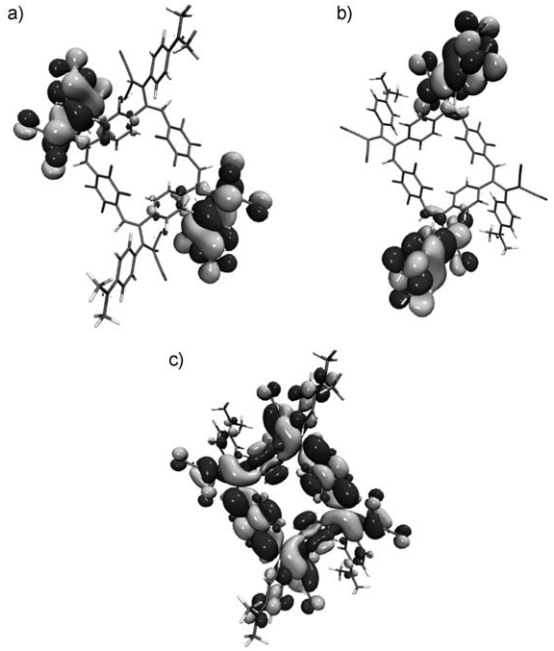

Figure 4. Representations of selected calculated molecular orbitals of cyclic $[AB]_2$ oligomer **16b**. a) HOMO; b) HOMO-3; c) LUMO.

(LUMO to LUMO+3) is delocalized over the entire cyclophane macrocycle with coefficients extending to the dicyanovinyl substituents (Figure 4c). Thus, the CT absorption band in the UV/Vis spectrum of cyclic oligomer **16b** arises from electron donation from the four anilino rings to the electron-accepting cyclophane macrocycle.

Conclusion

A series of model investigations enabled the identification of suitably reactive monomers, **12b** (A) and **9** (B), for the formation of regular [AB] oligomers by using the CA–CR reaction. In this novel oligomerization, nonplanar, push–pull buta-1,3-dienes with intense intramolecular CT interactions are formed in the chain-growth step. The use of pentafluorinated TCVB or DCVB substrates enables rate enhancements of 16- to 280-fold in the CA–CR reaction compared with reactions utilizing the non-fluorinated analogues; this facile reactivity was essential for obtaining oligomers. As shown in model reactions utilizing substrates containing either two cyanoolefin or two alkyne moieties, tricyanoolefins are less reactive than their dicyanovinyl counterparts; presumably, disfavorable steric effects negate the beneficial electron-withdrawing effects of the third CN group. Additionally, X-ray crystallographic studies enabled a detailed analysis of the influences of steric bulk on both molecular conformation and the efficiency of the intramolecular donor–acceptor conjugation in nonplanar donor-substituted cyanobuta-1,3-dienes.

CA–CR oligomerization between optimized monomers, A and B, which contain two DAA-acetylene and two DCV reactive sites, respectively, led to the formation of two types of oligomers with $[AB]_n$ or $B[AB]_n$ constitutions. Experimental results suggested that the $B[AB]_n$ oligomers were open-chain structures, whereas the $[AB]_n$ oligomers were macrocyclic structures. Further support for the macrocyclic structure of the $[AB]_2$ oligomer was obtained by computational investigations, which also showed that the observed intramolecular CT in this systems arose from electron donation from the peripheral dialkylanilino rings to the electron-deficient macrocycle. Future studies will be directed toward controlling the product distribution of the oligomerization reaction and exploring the supramolecular chemistry of the macrocyclic oligomers, which have been obtained by serendipity rather than by design. After further improving the reactivity of the monomeric starting materials by optimization of electronic and structural properties, new polymers and dendrimers should also become accessible.

Experimental Section

Materials and general methods: Reagents and solvents were purchased at reagent grade from Acros, Aldrich, and Fluka, and used as received. Compound **3** was commercially available. Compounds **1a**,[8a] **1b**,[13] **1c**,[14] **1d**,[15] **2a**,[13] **2b**,[13] **4**,[16] **5a**,[8a] **5c**,[8b] **9**,[2b] **12a**,[11] and **13a**[11] were synthesized according to literature procedures. The syntheses of compounds **2c**, **2d**, **12b**, and **13b** are described in the Supporting Information. General procedures for the [2+2] CA–CR and oligomerization reactions, as well as representative examples of these reactions, are given below; the syntheses and characterization data for compounds **5b**, **5d**, **6a**, **6b**, **7a–d**, **8a–d**, **11**, **14a**, **14b**, **15a**, **15b**, and oligomers **16c**, **16d** and **17a–d** are described in the Supporting Information. All reactions were performed in standard glassware under a positive pressure of Ar. TLC analysis was conducted on aluminum sheets coated with SiO_2 60 F_{254} obtained from Macherey–Nagel and visualized by UV irradiation (254 or 366 nm). Flash column chromatography (FC) was performed with SiO_2 60 (particle size 0.040–0.063 mm, 230–400 mesh ASTM; Fluka) or SiO_2 60 (particle size 0.063–0.200 mm, 70–230 mesh ASTM; Merck) and distilled technical solvents. Preparative TLC was performed by using SiliaPlate preparative plates (SiliCycle, 20×20 cm, thickness = 1000 μm). Melting points were measured on a Büchi B-540 melting-point apparatus in open capillaries and are uncorrected. ^1H, ^{13}C, and ^{19}F NMR spectra were recorded on Varian Gemini 300, Bruker DRX 400, Bruker DRX 500, or Bruker DRX 600 spectrometers at 298 K. Chemical shifts (δ) are reported in ppm relative to tetramethylsilane (TMS); the residual solvent peak was used as an internal reference. Coupling constants (J) are given in Hz. Apparent resonance multiplicities are described as s (singlet), brs (broad singlet), d (doublet), t (triplet), q (quartet), and m (multiplet). IR spectra were recorded on a Perkin–Elmer BX FT-IR spectrometer; signal designations: s (strong), m (medium), w (weak). All spectra were measured by using neat samples. UV/Vis spectra were recorded on a Varian Cary 500 spectrophotometer. The spectra were measured in CH_2Cl_2 in a quartz cuvette (1 cm) at 298 K. The absorption maxima (λ_{max}) are reported in nm with the extinction coefficient (ε [$M^{-1}cm^{-1}$]) in parentheses; shoulders are indicated as sh. Preparative recycling GPC was performed on a Japan Analytical Industries LC-9101 preparative recycling HPLC apparatus equipped with a Jaigel-2H column, using $CHCl_3$ (ReagentPlus grade, ≥99.8%) as the mobile phase, with a flow rate of 4 mL min^{-1}. Mass spectrometry was performed by the MS Service at ETH Zürich. High-resolution (HR) electron ionization (EI) mass spectra were measured on a Waters Micromass Auto-Spec Ultima spectrometer. HR matrix-assisted laser-desorption (MALDI) mass spectra were measured on a Varian IonSpec Ultima MALDI-FTICR mass spectrometer with 3-hydroxypyridine-2-carboxylic acid (3-HPA) as the matrix or on a Bruker Daltonicx Ultra-

flex II MALDI-TOF mass spectrometer using 2-[(2*E*)-3-(4-*tert*-butylphenyl)-2-methylprop-2-enylidene]malononitrile (DCTB) as matrix. Isotope signals with the highest relative abundance are reported. Elemental analyses were performed by the Mikrolabor at the Laboratorium für Organische Chemie, ETH Zürich, with a LECO CHN/900 instrument. The fluorine content was estimated by ion chromatography on a Metrohm 761 Compact IC instrument. In samples in which the presence of residual solvent was indicated by elemental analysis, its presence and identity was confirmed by ^{1}H NMR spectroscopy. Compound names were generated by using ACD/Lab 6.0 software (Advanced Chemistry Development).

General procedure for rate measurements: A 1-dram scintillation vial was charged with a solution of **3** (3.5 mg, 0.024 mmol) and hexamethylbenzene (1.3 mg, 0.0080 mmol) in $(CDCl_2)_2$ (0.75 mL). A given acceptor source (**1a** (3.7 mg), **1b** (5.9 mg), **2a** (4.3 mg), or **2b** (6.5 mg), 0.024 mmol) was added to this solution as a solid and dissolved. The resulting solution was then immediately transferred to an NMR tube. Single-scan ^{1}H NMR spectra were recorded at varying intervals (5–120 min) for the first 12 h on a Varian Gemini 300 spectrometer at 298 K. For the reactions using **1b**, **2a**, and **2b**, the collection of ^{1}H NMR spectra continued for seven half-lives; the reaction using **1a** was monitored to 25% conversion over 96 h.

Computational methods: All optimizations, frequency calculations, and vertical electronic transitions were calculated by using the Gaussian 09 program package.[17] Conformational analysis was performed by using a mixed Monte Carlo Multiple Minimum/Low-Mode Conformational Search method and the OPLS95 force field as implemented in MacroModel 9.7. All conformers with energies less than 3 kcal mol^{-1} relative to the global minimum were manually examined. Seven structures were selected for further optimization by using DFT at the B3LYP/6-31G(d) level of theory. This refinement yielded five conformers; harmonic vibrational analysis of these conformers performed at the same level of theory confirmed that all structures are minima of the potential energy surface. However, the global minimum was found to represent about 95% of the conformations in a Boltzmann distribution at 298.15 K. The UV/Vis spectrum of **16b** was simulated by using the structure of the global minimum. 100 vertical electronic transitions were computed at the TD CAM-B3LYP/6-31G(d) level of theory.

X-ray analysis: Unless otherwise noted, single crystals of indicated compounds were obtained by layering Me_2SO on top of a solution of the indicated compound in CH_2Cl_2 and allowing slow diffusion between the two layers at 22 °C. ORTEP diagrams of all compounds for which X-ray data was collected can be found in the Supporting Information. X-ray data collection was carried out on a Bruker KappaCCD diffractometer equipped with a graphite monochromator ($Mo_{K\alpha}$ radiation, λ = 0.71073 Å) and an Oxford Cryostream low-temperature device. Cell dimensions were obtained by least-squares refinement of all measured reflections (HKL, Scalepack[18a]), θ_{max} = 27.58. All structures were solved by direct methods (SIR97[18b]). All non-hydrogen atoms were refined anisotropically, hydrogen atoms were refined for compounds **1d**, **2c**, **4b**, **4d**, **7c**, and **7d** isotropically by full-matrix least-squares with SHELXL-97[18c] using experimental weights $(1/[\sigma^2(I_o)+(I_o+2I_c)^2/900])$. For compounds **2b**, **5a**, **5b**, **7a**, **7b**, **8c**, and **11**, hydrogen positions were calculated and included in the structure factor calculation.

X-ray crystal structure of **5b**: $C_{20}H_{12}F_5N_3$; M_r = 389.327; monoclinic; space group $P2_1/n$; ρ_{calcd} = 1.516 g cm^{-3}; Z = 4; a = 12.2399(8), b = 6.5379(5), c = 21.348(2) Å; α = 90.00, β = 93.111(4), γ = 90.00°; V = 1705.8(2) Å^3 at 123 K. Red brown needle (linear dimensions ca. 0.27 × 0.06 × 0.03 mm). Number of measured and unique reflections: 5711 and 2992, respectively (R_{int} = 0.093). Final $R(F)$ = 0.0638, $wR(F^2)$ = 0.1559 for 301 parameters and 2992 reflections with $I > 2\sigma(I)$ and $2.753 < \theta < 25.028$°.

X-ray crystal structure of **5d**: $C_{21}H_{16}F_3N_3$; M_r = 367.374; monoclinic; space group $P2_1/c$; ρ_{calcd} = 1.321 g cm^{-3}; Z = 4; a = 9.3457(4), b = 8.1316(4), c = 24.5171(12) Å; α = 90.00, β = 97.609(2), γ = 90.00°; V = 1846.8(2) Å^3 at 123 K. Colorless plate (linear dimensions ca. 0.18 × 0.06 × 0.03 mm). Number of measured and unique reflections: 4352 and 2501, respectively (R_{int} = 0.08). Final $R(F)$ = 0.0526, $wR(F^2)$ = 0.1379 for 308 parameters and 2501 reflections with $I > 2\sigma(I)$ and $2.425 < \theta < 22.986$°.

X-ray crystal structure of **6a**: $C_{21}H_{16}N_4$; M_r = 324.38; monoclinic; space group $P2_1/n$; ρ_{calcd} = 1.223 g cm^{-3}; Z = 4, a = 7.5396(11), b = 10.5438(12), c = 22.3962(15) Å; α = 90.00, β = 98.277(11), γ = 90.00°; V = 1761.86 Å^3 at 220(2) K. Orange cut fragment (linear dimensions ca. 0.21 × 0.18 × 0.17 mm). Number of measured and unique reflections: 6537 and 3596, respectively (R_{int} = 0.0287). Final $R(F)$ = 0.0489, $wR(F^2)$ = 0.1095 for 229 parameters and 3596 reflections with $I > 2\sigma(I)$ and $1.84 < \theta < 28.38$°.

X-ray crystal structure of **6b**: $C_{21}H_{11}F_5N_4$; M_r = 414.337; orthorhombic; space group $P2_12_12_1$; ρ_{calcd} = 1.524 g cm^{-3}; Z = 4; a = 6.4708(2), b = 14.0247(5), c = 19.9010(10) Å; α = 90.00, β = 90.00, γ = 90.00°; V = 1806.04(12) Å^3 at 173 K. Amber plate (linear dimensions ca. 0.36 × 0.27 × 0.027 mm). Number of measured and unique reflections: 3079 and 3063, respectively (R_{int} = 0.062). Final $R(F)$ = 0.1095, $wR(F^2)$ = 0.3100 for 274 parameters and 3063 reflections with $I > 2\sigma(I)$ and $2.753 < \theta < 25.028$°.

X-ray crystal structure of **7a**: $C_{26}H_{21}N_3$; M_r = 375.475; monoclinic; space group $P2_1/n$; ρ_{calcd} = 1.209 g cm^{-3}; Z = 4; a = 13.2760(4), b = 9.4253(3), c = 16.7739(4) Å; α = 90.00, β = 100.509(2), γ = 90.00°; V = 2063.71(10) Å^3 at 123 K. Dark yellow cube (linear dimensions ca. 0.18 × 0.18 × 0.15 mm). Number of measured and unique reflections: 8832 and 4704, respectively (R_{int} = 0.065). Final $R(F)$ = 0.0524, $wR(F^2)$ = 0.1402 for 264 parameters and 4704 reflections with $I > 2\sigma(I)$ and $2.753 < \theta < 27.485$°.

X-ray crystal structure of **7b**: $C_{26}H_{16}F_5N_3$; M_r = 465.425; triclinic; space group $P\bar{1}$; ρ_{calcd} = 1.436 g cm^{-3}; Z = 2; a = 9.4718(7), b = 10.0314(7), c = 12.5863(10) Å; α = 69.866(3), β = 83.756(3), γ = 73.520(4)°; V = 1076.60(14) Å^3 at 123 K. Amber cube (linear dimensions ca. 0.21 × 0.12 × 0.075 mm). Number of measured and unique reflections: 4953 and 2822, respectively (R_{int} = 0.108). Final $R(F)$ = 0.0697, $wR(F^2)$ = 0.1668 for 309 parameters and 2822 reflections with $I > 2\sigma(I)$ and $2.753 < \theta < 22.986$°.

X-ray crystal structure of **7c**: $C_{27}H_{20}N_4$; M_r = 400.485; triclinic; space group $P\bar{1}$; ρ_{calcd} = 1.237 g cm^{-3}; Z = 2; a = 8.6684(4), b = 10.3124(5), c = 13.4632(7) Å; α = 76.954(2), β = 88.910(2), γ = 66.933(2)°; V = 1075.46(9) Å^3 at 123 K. Amber plate (linear dimensions ca. 0.165 × 0.066 × 0.048 mm). Number of measured and unique reflections: 8540 and 3329, respectively (R_{int} = 0.066). Final $R(F)$ = 0.0555, $wR(F^2)$ = 0.1676 for 360 parameters and 4912 reflections with $I > 2\sigma(I)$ and $2.753 < \theta < 27.485$°.

X-ray crystal structure of **7d**: $C_{27}H_{20}F_3N_3$, M_r = 443.472; triclinic; space group $P\bar{1}$; ρ_{calcd} = 1.331 g cm^{-3}; Z = 2; a = 8.4794(3), b = 10.6526(4), c = 13.5062(5) Å; α = 87.982(2), β = 79.5732(14), γ = 67.358(2)°; V = 1106.57(7) Å^3 at 173 K. Pale yellow plate (linear dimensions ca. 0.36 × 0.24 × 0.039 mm). Number of measured and unique reflections: 8868 and 5047, respectively (R_{int} = 0.052). Final $R(F)$ = 0.0634, $wR(F^2)$ = 0.1962 for 378 parameters and 5047 reflections with $I > 2\sigma(I)$ and $2.753 < \theta < 27.485$°.

X-ray crystal structure of **8c**: Single crystals were obtained by layering hexanes on top of a solution of **8c** in tetrahydrofuran and allowing slow diffusion between the two layers at 22 °C. $C_{28}H_{19}N_5{\cdot}C_4H_8O$; M_r = 497.602; monoclinic; space group $P2_1/n$; ρ_{calcd} = 1.253 g cm^{-3}; Z = 4; a = 12.2364(5), b = 11.4908(5), c = 18.8308(9) Å; α = 90.00, β = 94.870(2), γ = 90.00°; V = 2638.2(2) Å^3 at 123 K. Red plate (linear dimensions ca. 0.22 × 0.18 × 0.03 mm). Number of measured and unique reflections 8518 and 4779, respectively (R_{int} = 0.060). Structure contains a disordered THF molecule in the asymmetric unit. Two atoms were refined over two positions. Final $R(F)$ = 0.0906, $wR(F^2)$ = 0.2419 for 342 parameters and 4779 reflections with $I > 2\sigma(I)$ and $2.425 < \theta < 25.350$°.

X-ray crystal structure of **11**: $C_{68}H_{74}N_8$; M_r = 1003.396; triclinic; space group $P\bar{1}$; ρ_{calcd} = 1.160 g cm^{-3}; Z = 1; a = 10.8650(4), b = 11.4737(4), c = 13.1850(2) Å; a = 111.005(2), β = 92.055(2), γ = 108.345(2)°; V = 1435.8(9) Å^3 at 123 K. Colorless cube (linear dimensions ca. 0.21 × 0.15 × 0.09 mm). Number of measured and unique reflections 8868 and 4701, respectively (R_{int} = 0.066). Two atoms of a hexyl chain are disordered and were refined over two positions. Final $R(F)$ = 0.0842, $wR(F^2)$ = 0.2251 for 365 parameters and 3634 reflections with $I > 2\sigma(I)$ and $2.753 < \theta < 24.407$°.

CCDC-802597 (**5b**), 802598 (**5d**), 802596 (**6a**), 802599 (**6b**), 802600 (**7a**), 802601 (**7b**), 802602 (**7c**), 802603 (**7d**), 802604 (**8c**), and 802605 (**11**) contain the supplementary crystallographic data for this publication. These

data can be obtained free of charge from The Cambridge Crystallographic Data Centre via www.ccdc.cam.ac.uk/data_request/cif.

General procedure for [2+2] CA–CR reactions: A solution of DAA-activated alkyne and electron-deficient olefin (DCVB, TCVB, or 1,4-divinylbenzene derivative) in DMF was stirred at 100 °C until complete conversion was observed by LC-MS. The solvent was evaporated, and the crude residue was washed with Et_2O. Purification by FC afforded the desired product.

*2,2′-{1,4-Phenylenebis[(1E)-3-[4-(dimethylamino)phenyl]-1-(pentafluorophenyl)-1-propen-2-yl-3-ylidene]} dimalononitrile (**10**)*: By using the general procedure, **1b** (25 mg, 0.10 mmol) and **9** (22 mg, 0.034 mmol) were stirred in DMF (2.5 mL) for 18 h. FC (SiO_2; toluene/hex 95:5) afforded **10** as a black solid (14 mg, 37 %). R_f = 0.86 (SiO_2; CH_2Cl_2); m.p. 241–243 °C; ^{1}H NMR (300 MHz, CD_2Cl_2): δ = 0.88 (t, J = 6.7 Hz, 12H), 1.29 (brs, 24H), 1.47–1.66 (m, 8H), 3.32 (t, J = 15.6 Hz, 8H), 6.60 (d, J = 9.4 Hz, 4H), 6.58 (s, 2H), 6.93 (s, 4H), 7.69 ppm (d, J = 9.3 Hz, 4H); ^{13}C NMR (75 MHz, CD_2Cl_2): δ = 14.2, 23.0, 27.0, 27.4, 31.9, 51.5, 78.9, 110.3–111.2 (m), 111.4, 115.0, 115.8, 119.0, 120.7, 128.4–129.2 (m), 128.8, 137.5, 137.8 (dm, ^1J(C,F) = 255.3 Hz), 144.2 (dm, ^1J(C,F) = 248.1 Hz), 145.8, 146.0, 152.4, 170.3 ppm; ^{19}F NMR (282 MHz, CD_2Cl_2): δ = −137.1 to −137.4 (m), −153.0 (t, J = 20.1 Hz), −161.1 to −161.4 ppm (m); IR (ATR): $\tilde{\nu}$ = 2925 (m), 2213 (m), 1599 (s), 1518 (m), 1491 (s), 1436 (m), 1412 (m), 1381 (m), 1335 (m), 1293 (m), 1178 (s), 975 (s), 909 (m), 821 (m), 704 (w), 636 cm^{-1} (w); UV/Vis (CH_2Cl_2): λ_{max} (ε) = 284 (31300), 348 (28500), 462 nm (53900 M^{-1}cm^{-1}); HR-MALDI-MS (3-HPA): m/z calcd for $C_{66}H_{67}F_{10}N_6^+$: 1133.5262; found: 1133.5278 $[M+H]^+$; elemental analysis calcd (%) for $C_{66}H_{66}F_{10}N_6$ (1133.27): C 69.95, H 5.87, N 7.42; found: C 70.12, H 6.06, N 7.23.

General procedure for synthesis of oligomers: Compounds **12b** (A) (100 mg, 0.155 mmol) and **9** (B) (46.9 mg, 0.155 mmol) were dissolved in TCE (10 mL) and the resulting mixture heated to 80 °C for 48 h. After cooling the mixture to room temperature, the solvent was removed and the residue was subjected to FC (SiO_2; CH_2Cl_2/EtOAc 99:1). The fractions containing oligomers were then subjected to recycling GPC (Jaigel-2H; $CHCl_3$) to afford the $[AB]_2$ oligomer **16b** as the major product (32 mg, 21 %), as well as small amounts of other oligomers, ranging from $B[AB]_1$ to $B[AB]_4$. $[AB]_2$ **(16b)**: m.p. 124–126 °C; ^{1}H NMR (600 MHz, $CDCl_3$): δ = 0.88–0.92 (m, 24H), 1.28–1.36 (m, 48H), 1.56–1.63 (m, 16H), 3.30–3.36 (m, 16H), 6.51 (s, 4H), 6.59 (d, J = 9.5 Hz, 8H), 7.21 (s, 8H), 7.73 ppm (d, J = 9.3 Hz, 8H); ^{13}C NMR (151 MHz, $CDCl_3$): δ = 14.1, 22.8, 26.8, 27.4, 31.7, 51.4, 74.1, 111.6, 114.9, 116.0, 119.8, 120.3, 129.2, 133.5, 137.7, 143.8, 144.9, 145.4, 152.4, 171.5 ppm; ^{19}F NMR (377 MHz, $CDCl_3$): δ = −136.2 ppm (s); IR (ATR): $\tilde{\nu}$ = 2926 (m), 2855 (m), 2214 (m), 1598 (w), 1536 (w), 1479 (s), 1410 (s), 1365 (m), 1332 (s), 1289 (s), 1199 (m), 1177 (s), 975 (s), 855 (m), 817(s), 735 (m), 676 cm^{-1} (m); UV/Vis (CH_2Cl_2): λ_{max} (ε) = 288 (72000), 461 nm (129900 M^{-1}cm^{-1}); MALDI-TOF-MS (DCTB): m/z (%): 1822 (65), 1823 (93), 1824 (61), 1825 (26), 1831 (78), 1832 (100) $[M-(C_6H_{12})+Na]^+$, 1833 (63), 1834 (23), 1893 (49), 1894 (61) $[M+H]^+$, 1895 (45), 1896 (22); HR-MALDI-MS (3-HPA) m/z calcd for $C_{120}H_{133}F_8N_{12}^+$: 1894.0643; found: 1894.0663 $[M+H]^+$.

Acknowledgements

Funding from an ERC Advanced Grant ("OPTELOMAC") is gratefully acknowledged. M.C. thanks the ETH Research Council for an ETH fellowship.

[1] a) J. M. Tour, *Chem. Rev.* **1996**, *96*, 537–553; b) Focus Issue on Organic Electronics: S. R. Forrest, M. E. Thompson, *J. Mater. Res.* **2004**, *19*, Issue 7; c) Special Issue on Organic Electronics and Optoelectronics: F. Faupaul, C. Dimitrakopoulos, A. Kahn, C. Wöll, *Chem. Rev.* **2007**, *107*, Issue 4.

[2] a) T. Michinobu, J. C. May, J. H. Lim, C. Boudon, J.-P. Gisselbrecht, P. Seiler, M. Gross, I. Biaggio, F. Diederich, *Chem. Commun.* **2005**, 737–739; b) T. Michinobu, C. Boudon, J.-P. Gisselbrecht, P. Seiler, B. Frank, N. N. P. Moonen, M. Gross, F. Diederich, *Chem. Eur. J.* **2006**, *12*, 1889–1905; c) M. Kivala, C. Boudon, J.-P. Gisselbrecht, P. Seiler, M. Gross, F. Diederich, *Chem. Commun.* **2007**, 4731–4733; d) P. Reutenauer, M. Kivala, P. D. Jarowski, C. Boudon, J.-P. Gisselbrecht, M. Gross, F. Diederich, *Chem. Commun.* **2007**, 4898–4900; e) M. Kivala, C. Boudon, J.-P. Gisselbrecht, B. Enko, P. Seiler, I. B. Müller, N. Langer, P. D. Jarowski, G. Gescheidt, F. Diederich, *Chem. Eur. J.* **2009**, *15*, 4111–4123; f) S.-i. Kato, M. Kivala, W. B. Schweizer, C. Boudon, J.-P. Gisselbrecht, F. Diederich, *Chem. Eur. J.* **2009**, *15*, 8687–8691; g) M. Jordan, M. Kivala, C. Boudon, J.-P. Gisselbrecht, W. B. Schweizer, P. Seiler, F. Diederich, *Chem. Asian J.* **2011**, *6*, 396–401.

[3] a) For the first observation of this transformation, see: M. I. Bruce, J. R. Rodgers, M. R. Snow, A. G. Swincer, *J. Chem. Soc. Chem. Commun.* **1981**, 271–272; b) K. Onitsuka, S. Takahashi, *J. Chem. Soc. Chem. Commun.* **1995**, 2095–2096; c) Y. Morioka, N. Yoshizawa, J.-i. Nishida, Y. Yamashita, *Chem. Lett.* **2004**, *33*, 1190–1191; d) P. Butler, A. R. Manning, C. J. McAdam, J. Simpson, *J. Organomet. Chem.* **2008**, *693*, 381–392; e) T. Shoji, S. Ito, K. Toyota, M. Yasunami, N. Morita, *Chem. Eur. J.* **2008**, *14*, 8398–8408.

[4] a) X. Wu, J. Wu, Y. Liu, A. K.-Y. Jen, *J. Am. Chem. Soc.* **1999**, *121*, 472–473; b) C. Cai, I. Liakatas, M.-S. Wong, M. Bösch, C. Bosshard, P. Günter, S. Concilio, N. Tirelli, U. W. Suter, *Org. Lett.* **1999**, *1*, 1847–1849; c) A. Galvan-Gonzalez, G. I. Stegeman, A. K.-Y. Jen, X. Wu, M. Canva, A. C. Kowalczyk, X. Q. Zhang, H. S. Lackritz, S. Marder, S. Thayumanavan, G. Levina, *J. Opt. Soc. Am. B* **2001**, *18*, 1846–1853.

[5] a) B. Esembeson, M. L. Scimeca, T. Michinobu, F. Diederich, I. Biaggio, *Adv. Mater.* **2008**, *20*, 4584–4587; b) C. Koos, P. Vorreau, T. Vallaitis, P. Dumon, W. Bogaerts, R. Baets, B. Esemberson, I. Biaggio, T. Michinobu, F. Diederich, W. Freude, J. Leuthold, *Nat. Photonics* **2009**, *3*, 216–219.

[6] a) T. Michinobu, H. Kumazawa, K. Noguchi, K. Shigehara, *Macromolecules* **2009**, *42*, 5903–5905; b) T. Michinobu, *Pure Appl. Chem.* **2010**, *82*, 1001–1009; c) Y. Li, K. Tsuboi, T. Michinobu, Y. Ishida, T. Hirai, T. Hayakawa, M.-a. Kakimoto, *J. Photopolym. Sci. Technol.* **2010**, *23*, 337–342.

[7] For the electronically controlled formation of regular oligomers by sequential CA–CR of electron-poor TCNE and electron-rich tetrathiafulvalene (TTF) to polyynes, see: a) M. Kivala, C. Boudon, J.-P. Gisselbrecht, P. Seiler, M. Gross, F. Diederich, *Angew. Chem.* **2007**, *119*, 6473–6477; *Angew. Chem. Int. Ed.* **2007**, *46*, 6357–6360; b) B. B. Frank, M. Kivala, B. Camafort Blanco, B. Breiten, W. B. Schweizer, P. R. Laporta, I. Biaggio, E. Jahnke, R. R. Tykwinski, C. Boudon, J.-P. Gisselbrecht, F. Diederich, *Eur. J. Org. Chem.* **2010**, 2487–2503.

[8] a) P. D. Jarowski, Y.-L. Wu, C. Boudon, J.-P. Gisselbrecht, M. Gross, W. B. Schweizer, F. Diederich, *Org. Biomol. Chem.* **2009**, *7*, 1312–1322; b) Y.-L. Wu, P. D. Jarowski, W. B. Schweizer, F. Diederich, *Chem. Eur. J.* **2010**, *16*, 202–211.

[9] a) Computational studies (B3LYP/6-32G(d) level) for the reaction between **1a** and **3** suggest that the transition state (TS) for the ring opening of the intermediate cyclobutene leading to the formation of the *s-cis*/*trans* intermediate is lower in energy by 8.2 kcal mol^{-1} than the TS leading to the *s-cis*/*cis* intermediate; Y.-L. Wu, unpublished results; b) M. Pomerantz, P. H. Hartman, *Tetrahedron Lett.* **1968**, *9*, 991–993; c) W. R. Dolbier, Jr., H. Koroniak, K. N. Houk, C. Sheu, *Acc. Chem. Res.* **1996**, *29*, 471–477; d) M. Murakami, Y. Miyamoto, Y. Ito, *J. Am. Chem. Soc.* **2001**, *123*, 6441–6442; e) M. Shindo, K. Matsumoto, S. Mori, K. Shishido, *J. Am. Chem. Soc.* **2002**, *124*, 6840–6841; f) M. Shindo, Y. Sato, T. Yoshikawa, R. Koretsune, K. Shishido, *J. Org. Chem.* **2004**, *69*, 3912–3916; g) J. M. Um, H. Xu, K. N. Houk, W. Tang, *J. Am. Chem. Soc.* **2009**, *131*, 6664–6665.

[10] a) C. Dehu, F. Meyers, J.-L. Brédas, *J. Am. Chem. Soc.* **1993**, *115*, 6198–6206; b) A. Hilger, J.-P. Gisselbrecht, R. R. Tykwinski, C. Boudon, M. Schreiber, R. E. Martin, H. P. Lüthi, M. Gross, F. Diederich, *J. Am. Chem. Soc.* **1997**, *119*, 2069–2078; c) N. N. P. Moonen, F. Diederich, *Org. Biomol. Chem.* **2004**, *2*, 2263–2266.

[11] P. M. Allemand, P. Delhaes, Z. G. Soos, M. Nowak, K. Hinkelmann, F. Wudl, *Synth. Met.* **1988**, *27*, 243–247.
[12] a) I. Tinoco, *J. Am. Chem. Soc.* **1960**, *82*, 4785–4790; b) J. C. Nelson, J. G. Saven, J. S. Moore, P. G. Wolynes, *Science* **1997**, *277*, 1793–1796; c) R. B. Prince, J. G. Saven, P. G. Wolynes, J. S. Moore, *J. Am. Chem. Soc.* **1999**, *121*, 3114–3121.
[13] M. D. Harvey, J. T. Pace, G. T. Yee, *Polyhedron* **2007**, *26*, 2037–2041.
[14] L. Horner, K. Klüpfel, *Justus Liebigs Ann. Chem.* **1955**, *591*, 69–98.
[15] L. C. W. Chang, J. von Frijtag Drab. Jacobien, T. Mulder-Krieger, R. F. Spanjersberg, S. F. Roerink, G. van den Hout, M. W. Beukers, J. Brussee, A. P. IJzerman, *J. Med. Chem.* **2005**, *48*, 2045–2053.
[16] M. Rubin, A. Trofimov, V. Gevorgyan, *J. Am. Chem. Soc.* **2005**, *127*, 10243–10349.
[17] Gaussian 09, Revision A.02, M. J. Frisch, G. W. Trucks, H. B. Schlegel, G. E. Scuseria, M. A. Robb, J. R. Cheeseman, G. Scalmani, V. Barone, B. Mennucci, G. A. Petersson, H. Nakatsuji, M. Caricato, X. Li, H. P. Hratchian, A. F. Izmaylov, J. Bloino, G. Zheng, J. L. Sonnenberg, M. Hada, M. Ehara, K. Toyota, R. Fukuda, J. Hasegawa, M. Ishida, T. Nakajima, Y. Honda, O. Kitao, H. Nakai, T. Vreven, J. A. Montgomery, Jr., J. E. Peralta, F. Ogliaro, M. Bearpark, J. J. Heyd, E. Brothers, K. N. Kudin, V. N. Staroverov, R. Kobayashi, J. Normand, K. Raghavachari, A. Rendell, J. C. Burant, S. S. Iyengar, J. Tomasi, M. Cossi, N. Rega, J. M. Millam, M. Klene, J. E. Knox, J. B. Cross, V. Bakken, C. Adamo, J. Jaramillo, R. Gomperts, R. E. Stratmann, O. Yazyev, A. J. Austin, R. Cammi, C. Pomelli, J. W. Ochterski, R. L. Martin, K. Morokuma, V. G. Zakrzewski, G. A. Voth, P. Salvador, J. J. Dannenberg, S. Dapprich, A. D. Daniels, Ö. Farkas, J. B. Foresman, J. V. Ortiz, J. Cioslowski, D. J. Fox, Gaussian, Inc., Wallingford CT, **2009**.
[18] a) Z. Otwinowski, W. Minor, *Methods Enzymol.* **1997**, *276*, 307–326; b) A. Altomare, M. C. Burla, M. Camalli, G. L. Cascarano, C. Giacovazzo, A. Guagliardi, A. G. G. Moliterni, G. Polidori, R. Spagna, *J. Appl. Crystallogr.* **1999**, *32*, 115–119; c) G. M. Sheldrick, *Acta Crystallogr. A* **2007**, *64*, 112–122.

Received: December 20, 2010
Revised: February 2, 2011
Published online: April 18, 2011

